Biofabrication of a tri-layered 3D-bioprinted CSC-based malignant melanoma model for personalized cancer treatment

Biofabrication

PAPER

Biofabrication of a tri-layered 3D-bioprinted CSC-based malignant melanoma model for personalized cancer treatment

Julia López de Andrés[1,2,3,6,8], Marta Ruiz-Toranzo[1], Cristina Antich[4], Carlos Chocarro-Wrona[7], Elena López-Ruíz[1,2,3,5,8], Gema Jiménez[1,2,3,6,8,*] and Juan Antonio Marchal[1,2,3,6,8,*]

[1] Biopathology and Regenerative Medicine Institute (IBIMER), Centre for Biomedical Research (CIBM), University of Granada, Granada, 18100, Spain
[2] Instituto de Investigación Biosanitaria ibs.GRANADA, University Hospitals of Granada- University of Granada, Granada, 18100, Spain
[3] Excellence Research Unit 'Modeling Nature' (MNat), University of Granada, Granada, 18100, Spain
[4] National Center for Advancing Translational Sciences, National Institute of Health, 28050 Rockville, MD, United States of America
[5] Department of Health Sciences, University of Jaén, 23071 Jaen, Spain
[6] Department of Human Anatomy and Embryology, Faculty of Medicine, University of Granada, Granada, 18016, Spain
[7] 3d.FAB, L'Institut de Chimie et Biochimie Moléculaires et Supramoléculaires (ICBMS)-GEMBAS, Université Lyon 1, Villeurbanne 69100, France
[8] BioFab i3D Lab- Biofabrication and 3D (bio)printing Singular Laboratory, University of Granada, Granada 18100, Spain
[*] Authors to whom any correspondence should be addressed.

E-mail: gemajg@ugr.es and jmarchal@ugr.es

Keywords: 3D bioprinting, tumor microenvironment, malignant melanoma, tumor model, melanoma 3D model

Supplementary material for this article is available online

OPEN ACCESS

RECEIVED
22 February 2022

REVISED
19 May 2022

ACCEPTED FOR PUBLICATION
30 August 2022

PUBLISHED
15 May 2023

Abstract

Conventional *in vitro* cancer models do not accurately reproduce the tumor microenvironment (TME), so three-dimensional (3D)-bioprinting represents an excellent tool to overcome their limitations. Here, two multicellular tri-layered malignant melanoma (MM) models composed by cancer stem cells (CSCs) isolated from a MM established cell line or a primary-patient derived cell line, fibroblasts, mesenchymal stem cells, and endothelial cells, embedded within an agarose-collagen type I hydrogel were bioprinted. Embedded-cells showed high proliferation and metabolic activity, and actively remodeled their TME. MM hydrogels displayed similar rheological properties that skin and were able to support an early onset of vascularization. Besides, MM hydrogels displayed different response to vemurafenib compared with cell cultures, and supported tumorigenesis in murine xenotransplant achieving more mimetic *in vivo* models. For the first time a tri-layered 3D-bioprinted CSC-based human MM model is developed recreating TME *in vitro* and *in vivo* and response to treatment, being useful for precision treatment regimens against MM.

Abbreviations

αSMA	Alpha smooth muscle actin
AFM	Atomic force microscopy
ALDH1	Aldehyde dehydrogenase 1
CSCs	Cancer stem cells
CTG	Cell Tracker Green
CTR	Cell Tracker Red
DEAB	N,N-diethylaminobenzaldehyde
ECs	Endothelial cells
ECM	Extra-cellular matrix
ESEM	Environmental scanning electron microscopy
FAPα	Fibroblast activation protein alpha
FBs	Fetal bovine serum
FBS	Human fibroblasts
HUVECs	Human umbilical vein endothelial cells
KTCs	Human keratinocytes
MM	Malignant melanoma
MSCs	Mesenchymal stem cells
NSG	NOD scid gamma
PDX	Patient derived xenograft
PBS	Phosphate-buffered saline
qPCR	quantitative polymerase chain reaction
RT	Room temperature
SEM	Scanning electron microscopy
TEM	Transmission electron microscopy
TME	Tumor microenvironment
VEGF	Vascular endothelial growth factor
VMF	Vemurafenib

1. Introduction

MM, the deadliest form of skin cancer, is currently a major public health concern, due to its rate of increase is higher than for any other solid cancer

types, with more than 300 000 new diagnosed cases in 2020 (GLOBOCAN). Despite the most prevalent types of cancer share common characteristics such as high proliferation rates or invasion capability, each one has a unique TME [1]. TME is comprised of a complex and dynamic network that continually changes its composition and state [2]. Apart from tumor cells, TME is composed of multipotent stromal cells/MSCs, FBs, blood vessels, endothelial precursor cells, immune cells, and secreted factors such as cytokines and growth factors [3]. Literature strongly supports that these microenvironment features are crucial for the recapitulation of native tumor behavior [3]. Furthermore, it has been described that a small cell subpopulation of CSCs within the tumor mass largely controls the TME and tumor progression. Indeed, CSCs are responsible for pharmacological resistance and subsequent tumor recurrence in patients, making them an indispensable therapeutic target in cancer research [4].

Traditional culture models for cancer research fail to fully recreate the TME, either mimetic cell-cell or cell-matrix interactions, tumor vascularization, and many of the known characteristics of tumors *in vivo* [1, 5]. Three-dimensional (3D) tumor models including a biomimetic ECM have achieved more accurate representations of cancer tissues in terms of TME and biological behavior [5], essential for developing early diagnosis and treatment strategies for cancer. Microextrusion-based 3D bioprinting represents the optimal technique to obtain a tumor equivalent, since the heterogeneity and complexity of TME can be replicated by co-printing several cell types, ECM, and biomolecules laden in different bioinks, in a well-organized spatial distribution [1, 6]. Hydrogels provide perfect soft material systems to mimic native ECM microenvironments [7], supports cell viability and proliferation [8, 9], and offer more efficient, scalable and repeatable 3D models [5, 10]. Collagen type I is the most common hydrogel matrix for skin and tumor 3D modeling [11–13], as it supports cell attachment and migration allowing growth and function of several cell types [14, 15]. When used for 3D bioprinting, collagen can be combined with other ECM components such as hyaluronic acid [16], in order to obtain more printable bioinks.

To recreate and bioprint a reliable MM model not only the bioink but also the structure has to be carefully designed. Skin is a very complex organ, composed of different cell types and organized in three layers (epidermis, dermis and hypodermis). The epidermis is fundamentally composed of keratin-producing KTCs and melanocytes; the dermis highlights for its collagen and elastic fibers-producing FBs and the hypodermis is formed of adipocytes and connective tissue [17]. 3D bioprinting has been applied to successfully engineer the stratified human skin [18, 19], allowing to bridge the gap between *in vitro* and clinical testing [20].

In the present study, we have biofabricated a 3D bioprinted CSCs-based human MM model using both a primary patient-derived MM and established MM cell lines. In order to recapitulate the MM microenvironment, bioinks based on a matrix of collagen type I and agarose were prepared by combining MM CSCs and KTCs for the epidermal layer, HUVECs and FBs for the dermal layer and MSCs for the hypodermal layer. After bioprinting, the constructs were mechanical and functionally characterized and their response to the chemotherapeutic VMF was tested. In addition, we established xenograft models by implanting the MM-hydrogels subcutaneously in mice, to analyze their ability to faithful recreate the molecular and pathological features of human melanoma *in vivo*.

2. Material and methods

2.1. Cell cultures

The human MM established cell line A A375 (ATCC® CRL-1619) and HUVECs (ATCC® CRL-1730TM) were obtained from American Type Culture Collection. KTCs were obtained from ScienCell (ScienCell; number 2110). The human melanoma primary patient-derived cell line Mel-1 comes from a malignant metastatic melanoma (stage M1a) skin biopsy and was provided by the Biobank of the Andalusian Public Health System (Spain). MSCs and FBs were isolated from skin tissue (ethics committee reference: 0467N-20). For enrichment of CSCs, tumor cells were cultured on low-adherent surface and serum-free conditions, conforming melanospheres. HUVECs-FBs spheroids were performed following the hanging-drop method. Cell lines isolation and culture protocols are detailed in supplementary data.

2.2. Cell characterization

MSCs, FBs and CSCs were characterized by flow cytometry and differentiation assay, detailed in Supplementary data.

2.3. Cell-laden hydrogel biofabrication

Agarose solution (3.3% w/v) was prepared by dissolving Agarose UltraPureTM Low Melting Point (Thermo ScientificTM) powder in PBS. The solution was maintained at 4 °C, and pre-heated at 40 °C before used, in order to keep it liquid for the printing process. Collagen type I solution (3.58 mg ml^{-1} rat tail collagen, Corning) was neutralized with 1 M $NaCHO_3$ just before printing. To prepare the bioink, properly volumes of agarose and collagen were mixed to obtain 1.5% agarose and 1.5 mg ml^{-1} collagen concentrations.

2.3.1. CSCs- based bioink for proliferation assay

Melanospheres were collected on PBS and centrifuged. Isolated CSCs were obtained by harvesting melanospheres with trypsin-EDTA (0.25%, Sigma

Aldrich) in order to dissociate them into single cells. Each pellet was carefully mixed with collagen type I and agarose homogenously. The final cell-laden bioink was then loaded into a sterile 3 ml thermal syringe, previously heated at 37 °C to avoid a thermal shock.

2.3.2. Cell-laden bioinks for MM hydrogels

MSCs, FBs and KTCs in culture flasks were harvested with trypsin (0.25%, Sigma Aldrich), and centrifuged. CSCs melanospheres were also collected and centrifuged. After centrifugation, cell pellets were loaded into the syringe as described in section 2.3.1. Cells concentration for all the models were: CSCs melanospheres (cell density of 3×10^6 cells ml^{-1}, amounting to between 1200 and 1800 melanospheres), KTCs (cell density of 3×10^6 cells ml^{-1}), FBs, HUVECs, and MSCS (cell density of 1.5×10^6 cells ml^{-1}), placed in different contiguous layers (from top to bottom) simulating the three-layered MM skin structure, so loaded in their correspondents' syringes.

2.4. Bioprinting procedure

MM hydrogels were bioprinted by an extrusion-based REGEMAT 3D V1 bioprinter (REGEMAT 3D, Granada, Spain). Bioprinting parameters were programmed employing the Regemat 3D's software: flow speed 12 mm s^{-1}, pore size 0.6 mm^2, nine layers (height 0.21 mm), infill pattern diagonal (45°), width 10 mm, length 10 mm, syringe temperature 40 °C (figure S1). For extrusion, a plastic needle (TT22-DHUV-1000) was used. Different models were designed and bioprinted in this study, as shown figure S2: (a) CSCs-loaded hydrogels both as melanospheres or individualized; (b) trilaminar MM hydrogels including CSCs, FBs, MSCs and KTCs, (c) MM hydrogels loading HUVECs-FBs spheroids on the dermal layer. Once prepared the different bioinks and loaded into the thermal syringes, they were placed into the bioprinter and the process was initiated. The printed constructs quickly gelled after printing, and were placed into ultra-low adherence 12-well plates (Corning) and maintained for 14 days under cell culture conditions at 37 °C in a 5% CO_2 atmosphere. About 1 ml of corresponding fresh medium was added and replaced every three days.

2.5. Hydrogel structure and cell activity analysis

MM hydrogels structure and viability assays were analyzed by confocal microscopy. Cell proliferation was measured using Alamarblue® assay (Bio-Rad Laboratories, Inc. manufactured by Trek Diagnostic Systems. U.S). For ultrastructural analysis, MM hydrogels were imaged with the ESEM (QuemScan650F). For extracellular vesicles (EVs) extraction, the MM hydrogels were cultured during 14 days, using heat-inactivated exosome-depleted FBS, which was depleted of bovine exosomes by ultracentrifugation at 100 000 g for 70 min. The conditioned media was collected and centrifuged for 20 min at 10 000 g to remove cell debris and then centrifuged for 80 min at 100 000 g to isolated the EVs. Finally, the pellet obtained was washed with PBS and centrifuged again for 80 min at 100 000 g. The final pellet was diluted in PBS. EVs were imaged with LIBRA 120 PLUS TEM (Carl Zeiss SMT, Oberkochen, Germany), SEM (HITACHI, S-510), and NX20 atomic force microscopy (Park Systems, Suwon, South Korea). For TEM and SEM analysis, the EVs were further negatively stained with uracil acetate on a carbon membrane. Exosome size analysis were performed on NanoSight NS500 Instruments (Malvern Instruments, Malvern, UK). Presence of Alix marker was performed by Western-Blot. Phenotypic study of CSCs and FBs in the hydrogel MM was performed by immunofluorescence of αSMA, FAPα, CD44 and ALDEFLUOR. Images were taken by confocal microscopy (Nikon Eclipse Ti-E A1, USA) and analyzed using Image J Software. Detailed protocols are described in supplementary data.

2.6. Rheology

The rheological tests were carried out in a torsional rheometer MCR302 (Anton Paar, Austria) at 25 °C, which was used to quantify Young's and viscoelasticity modulus, as detailed in supplementary data.

2.7. Vasculature assays

For VEGF-effect evaluation, MM hydrogels containing isolated HUVECs and FBs were kept in medium supplemented with VEGF (250 ng ml^{-1}) or without VEGF for two weeks. MM-hydrogels were analyzed immunohistochemically, as detailed in supplementary data. Images were taken by confocal microscopy (Nikon Eclipse Ti-E A1, USA) and analyzed using Image J Software.

2.8. Effect of VMF in the tumor model

The drug VMF was tested on CSCs melanospheres culture and on CSCs-loaded hydrogels for the two tumor cell lines, A375 and Mel-1, and in the MM hydrogels loaded with CSCs, FBs and MSCs. Following the protocols described in section 2.5, proliferation assay by AlamarBlue® was used to determine the effect of VMF on melanospheres cultured in suspension and CSCs-loaded hydrogels. To test the effect on MM hydrogels, cell viability was analyzed using the Live/Dead kit (ThermoFisher). The doses administered for the A375 cell line were 0 μM, 0.0072 μM, 0.036, 0.072 μM and 0 μM. The doses administered for the Mel-1 cell line were 0 μM, 0.508 μM, 2.54 μM, 5.08 μM, and 10 μM. The drug was refreshed every 24 h.

2.9. qPCR analysis of ABC genes

Gene expression levels for ABCG2, ABCB1, ABCC2, ABCC3 and ABCB5 were quantified by quantitative polymerase chain reaction (qPCR), as described in supplementary data.

2.10. *In vivo* study

NOD scid gamma (NSG) mice were used to establish xenograft tumors ($n = 6$ for each condition). They were housed and maintained at 20 °C–24 °C, 50% relative humidity, a 14–10 h light-dark cycle with food and water ad libitum. The tumors were generated by: (a) subcutaneous injections of A375 individualized CSCs at 5×10^5 cells/mouse embedded in Matrigel Matrix (Corning) using 26-gauge needles (Matrigel control); and (b) subcutaneous implantation of 0.5 ml A375 CSCs-loaded hydrogel or MM hydrogel (loading 5×10^5 CSCs, and 2.5×10^5 FBs, HUVECs and MSCs), with a size of 0.6 cm width and 0.2 cm height. Tumor growth was measured every four days using a digital caliper, and the tumor volume was calculated by the formula $V = \text{length}^2 \times \text{width} \times \pi/6$. After 34 days, the tumors were sectioned and prepared for immunohistochemical assays, as described in detail in supplementary data. All the procedures were approved by the Institutional Animal Care and Use Committee at the University of Granada (ethics committee reference: 13/08/2020/095). The images were obtained using Leica DM 550B microscope.

2.11. Statistical analysis

Results presented in this work are represented as mean ± SEM from at least three replicas. ANOVA test was used to determine data normality. Two-tailed Student's t-test was used to determine test significance between different hydrogels or conditions. Results were considered statistically significantly different at $^{*}p < 0.05$, $^{**}p < 0.01$ and $^{***}p < 0.005$.

3. Results

3.1. Cell viability and characterization of trilaminar MM models

To closely mimic an MM environment a trilaminar hydrogel was engineered, establishing the proper bioprinting protocol. First, MSCs and FBs were isolated from human skin tissue obtained during abdominoplasty surgery and correctly characterized (see supplementary material, figure S4) [21]. Furthermore, CSCs from established A375 and primary patient-derived Mel-1MM cell lines were obtained and characterized (see supplementary material, figure S5), and the optimal culture condition of the CSCs-loaded hydrogels was defined (see supplementary material, figure S6).

To obtain the MM hydrogels, a first layer of MSCs was printed followed by a layer of FBs, and a last one of Mel-1 or A375 CSCs; all these cells embedded in a mixture of 1.5 mg ml^{-1} collagen type I and 1.5% agarose (described in more detail in section 2.4). To test the degradation, images of the bioprinted tumor were taken at days 1 and 14 showing that hydrogels maintained a length side of 1.2 cm, showing no modifications in the shape during two weeks (figure S6(C)). In order to follow the maintenance of the layered structure, CSCs and MSCs were pre-stained with CTG CMFDA dye to visualize epidermal and hypodermal layers, and FBs with CellTracker Red CMFDA (CTR) to stain the dermal layer. Confocal micrographs showed that the MM hydrogels were able to maintain their trilaminar structure over time (figures 1(A) and S6(D)) evidencing the correct consistence and desirable properties of the agarose- and collagen type I-based bioink.

Bioprinting process could affect to cell viability due to the high shear stress at the nozzle, so live/dead assay was performed at days 1 and 14 of culture (figure 1(B)). Twenty-four hours after the bioprinting process cells displayed a high viability and homogenous distribution among the three layers with a remarkable staining in viable cells (green) respect to death cells (red). Moreover, no significant differences on living cells percentages were found between day 1 and day 14. To corroborate these results, proliferation of MM hydrogels was measured with Alamarblue® until day 14 (figure 1(B)). In both MM hydrogels, statistical analysis showed a significant increment ($^{***}p < 0.005$) on cell proliferation rate from day 1 forward. Mel-1MM hydrogels maintained a constant proliferation rate from day 3 to day 14, while A375 MM hydrogels showed a significant increase in proliferation rate at day 14 compared to day 10 ($^{***}p < 0.005$).

Due to the high heterogeneity of melanoma CSCs, the differentiation status of hydrogel-embedded tumor cells was finally analyzed after 14 days of culture, using the membrane marker CD44, widely described for this subpopulation [22, 23], and ALDH activity, whose overexpression has also been strongly associated with an undifferentiated state of tumor cells [22, 24] (see supplementary material, figure S5). As a negative control, we applied N,N-diethylaminobenzaldehyde (DEAB) to the MM hydrogels, an inhibitor of the ALDH enzyme. It can be observed that after 24 h in culture, A375 and Mel-1 cells present a stem state, with a percentage of the almost total population expressing the CD44 marker (figure S5(C)). In addition, they also present enhanced ALDH activity, higher in A375 than in Mel-1, consistent with the results of the cytometry previously performed on melanospheres (figure S5). After 14 days in culture, cell populations of both lines maintained the stemness phenotype, this being more evident for the A375 cell line. These results agree with the MM hydrogels proliferation rates (figure 1), in which it is noted that Mel-1MM hydrogels have a higher growth rate than those loaded with A375, an indicator of cell differentiation since stem cells are

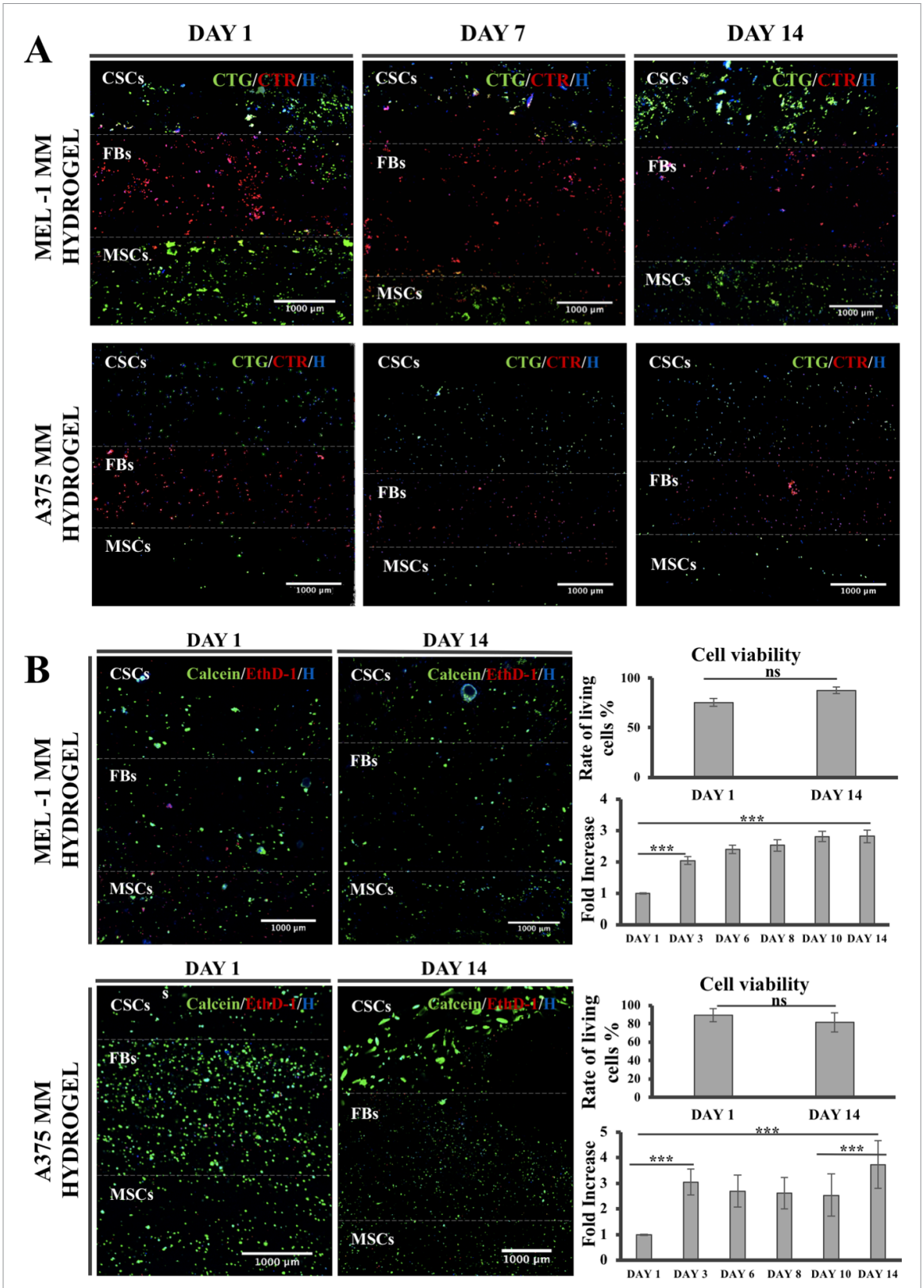

Figure 1. Cellular structure, viability and proliferation of MM hydrogels. (A) Confocal representative images of 10z stacks obtained by confocal microscopy showing a cross-section of the printed 3D Mel-1 or A375 MM hydrogels after 1, 7 and 14 days in culture. Scale bar: 1000 μm; volume height 80 μm. CSCs and MSCs were stained with CellTracker Green CMFDA (green) and FBs were stained with CellTracker Red CMFDA (red) and Hoechst (blue). Scale bars: 50 μm (Mel-1 model) and 100 μm (A375 model). (B) Confocal representative images of 10z stacks at days 1 and 14 of Mel-1MM hydrogel and A375 MM hydrogel. Live cells are shown in green (Calcein) and dead cells in red (EthD-1). Scale bar: 1000 μm. Graphics show quantification of live/dead cells percent at days 1 and 14 with no significant differences on living cells fraction ($n = 4$; $p > 0.05$) and fold changes in proliferation of cells (performed with Alamarblue®) embedded in the MM hydrogels at days 1, 3, 6, 8, 10 and 14, respectively ($n = 4$; $p < 0.005$).

characterized by a lower proliferation (4). Thus, in both cases, there is a heterogeneous representation of tumor cells in the TME.

3.2. Ultrastructural hydrogel characterization

In order to characterize the microstructure of the MM hydrogels, an ESEM was performed after 14 days in culture. Although an irregular fibrillar pattern was observed on the surface (figure 2(Aa)), after cutting transversely the hydrogel, a dense network of fibrils was discerned with porous of irregular shape ranging between 2 and 3 μm in diameter and fibers with a thickness of 70–140 nm (figure 2(Ab-c)). Cell analysis showed that MM CSCs were forming melanospheres on the top hydrogel layer (epidermis) and MSCs and FBs were found on the middle and bottom layers (dermis and hypodermis, respectively) (figure 2(B)). Also, signs of intercellular communication were observed as showed EVs secretion (figure 2(C)), ranging from about 80 nm to vesicles of about 500 nm (figure 2(Ca), red arrows), sizes that corresponds with exosomes and microvesicles, which were found dispersed in the hydrogel (figure 2(Cb), red arrows). Furthermore, the model displayed high cell metabolic activity as suggest cell division (figure 2(Cb), white arrow), and the production of a dense material that covered the fiber networks, indicating ECM secretion and the remodeling of their own extracellular microenvironments (figure 2(Ca), white arrow, and figure 2(Cc)).

3.3. Rheological properties of MM hydrogels

Changes in mechanical properties of ECM are essential for tumor progression. Thus, we used rheological tests to measure the mechanical properties of the MM hydrogel over time in culture. Figure 2(D) illustrates the viscoelastic moduli of hydrogels containing cell-free layers, only one cell-laden layer: MSCs-layer, FBs-layer, CSCs melanospheres-layer (composed of Mel-1 or A375 cells); or containing the three cell-laden layers together, called MM hydrogel (MSCs, FBs, and CSCs melanospheres-layers). Independent on cell composition, the storage modulus of all the hydrogels remained always larger than the loss modulus, evidencing the existence of a gel-like structure. Initially, the range was between 2666 772 and 5335 611 Pa for G′ and 148 and 245 Pa for G″, without significant differences among cell-type used and with cell-free hydrogels. All these values were comparable to those of healthy human skin tissue used as control (2945 767 Pa and 632 Pa for G′ and G″, respectively). At day 10, it was observed a significant decrease in viscoelastic moduli of CSCs-loaded hydrogels while in MM hydrogels and hydrogels embedding non-cancerous cell-layers this phenomenon was notable later (at day 20). The viscoelastic moduli from CSCs-loaded hydrogels were recovered again by day 20, raising G′ values of 3359 583 and 2666 111 Pa, for Mel-1 and A375 melanosphere, respectively. In figure 2(E), it is shown the compression moduli of the hydrogels with different cell composition. As it is observed, the incorporation of cells did not increase the Young moduli in the hydrogels, except for MM hydrogels. Similar to viscoelastic moduli, the values of hydrogels with different cell composition decreased significantly after culture period, being clearly faster in those containing CSCs melanospheres-layer. Measurement from MM and CSCs-loaded hydrogels revealed significant differences in stiffness by day 10, exhibiting values of 533 825 and 908 916 Pa, respectively. These compression values were increased from day 10 to day 20, in the case of CSCs-loaded hydrogels, although differences were not significant.

3.4. Cell communications within the MM hydrogels

In order to confirm the secretion of EVs from the cells embedded in the model, conditioned media was collected from MM hydrogels, and the EVs were isolated and then analyzed by different techniques (figures 3(A)–(D)).

NanoSight analyses show for both A375 and Mel-1MM hydrogels the presence of vesicles of different sizes, ranging from 25–50 nm to 500–600 nm (figure 3(A)). It was also confirmed by different microscopy techniques: TEM (figure 3(B)), SEM (figure 3(B)), and AFM (figure 3(C)), showing the EVs diameters coincide with the ranges previously reported. Indeed, the size of several EVs indicates the presence of exosomes, since many EVs measured between 20 and 80 nm, so it was confirmed by WB the expression of the exosome marker Alix [25], positive again for both models (figure 3(D)).

Furthermore, it was performed an analysis of the phenotype of the FBs included in the model, since it has been described how these undergo a phenotypic change to cancer-associated fibroblast (CAFs) when co-cultured with tumor cells, and to a greater degree with CSC [14]. To this end, the MM hydrogels were stained with αSMA and FAPα antibodies, widely used for the characterization of CAFs [14, 26], after 1 and 14 days in culture (figure 3(E)). Immunofluorescence images show that while no significant change in αSMA expression is discernible, there is a marked increase in FAPα expression by FBs after 14 days in culture. Both EVs secretion and FBs phenotype change, strongly support that the cells included in the MM hydrogel are able to actively communicate with each other.

3.5. Induction of vascularization in the MM hydrogels

The vasculature is an essential element of the TME since it provides access to nutrients and oxygen, and

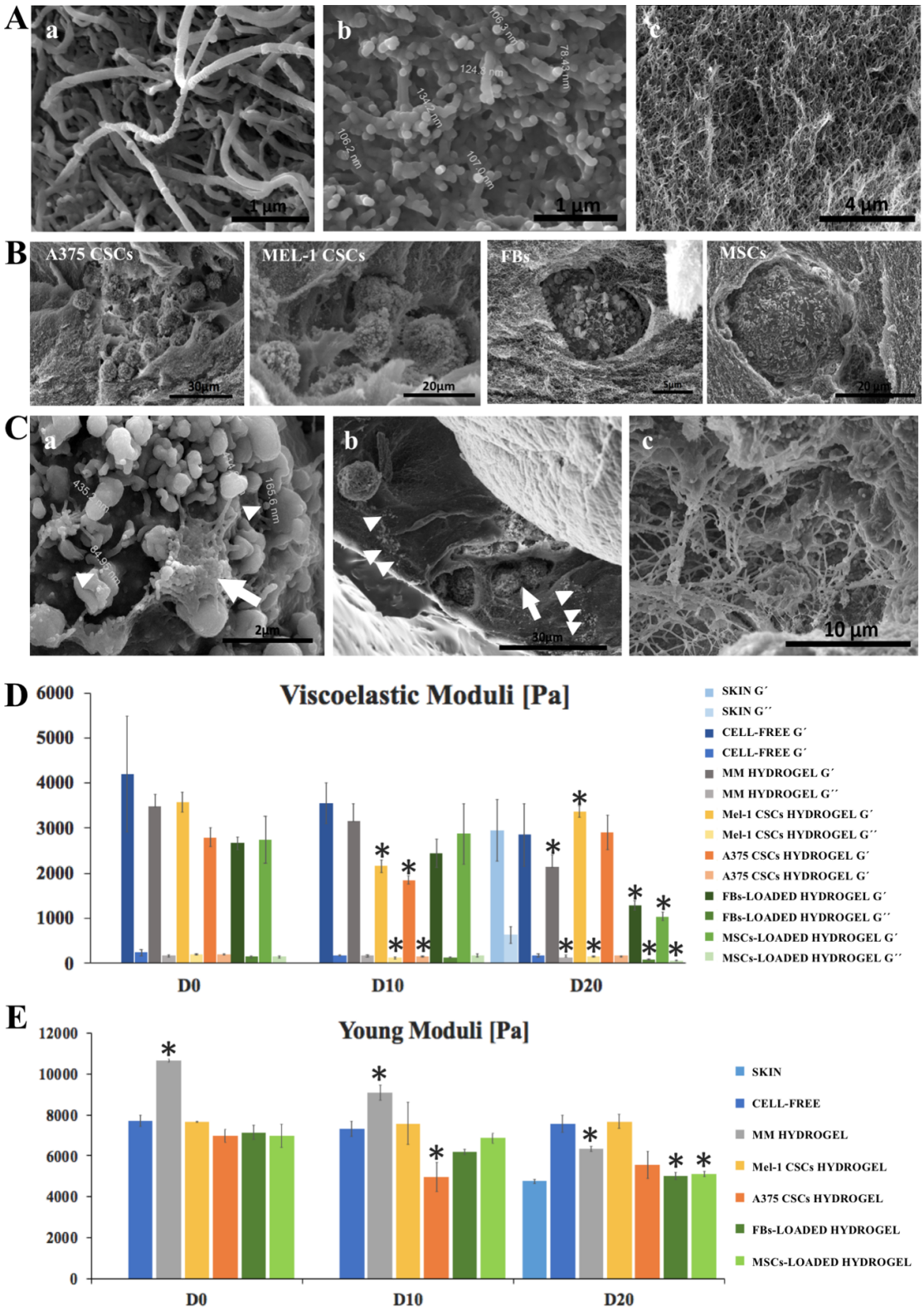

Figure 2. Ultrastructural and rheological analysis of cell-free and cell-laden MM hydrogels. ESEM images of (A) cell-free hydrogel fibers on the surface (a) and hydrogel fiber network observed transversely (b), (c); (B) A375 CSCs, Mel-1 CSCs, MSCs and FBs embedded in the MM hydrogel; and (C) cellular activity samples including secretion of different sized microvesicles and exosomes ((a), (b), red arrows), cellular division ((b), white arrow) or synthesis of new extracellular matrix ((a) white arrow, (c)). Viscoelastic moduli (D) and Young moduli (E) of MM hydrogels containing cell-free layers, only one cell-laden layer: MSCs-layer, FBs-layer, CSCs melanospheres -layer (composed of Mel-1 or A375 cells) or containing the three cell-laden layers together (MSCs, FBs, and CSCs melanospheres-layers), called trilaminar, after 0, 10 and 20 days on culture.

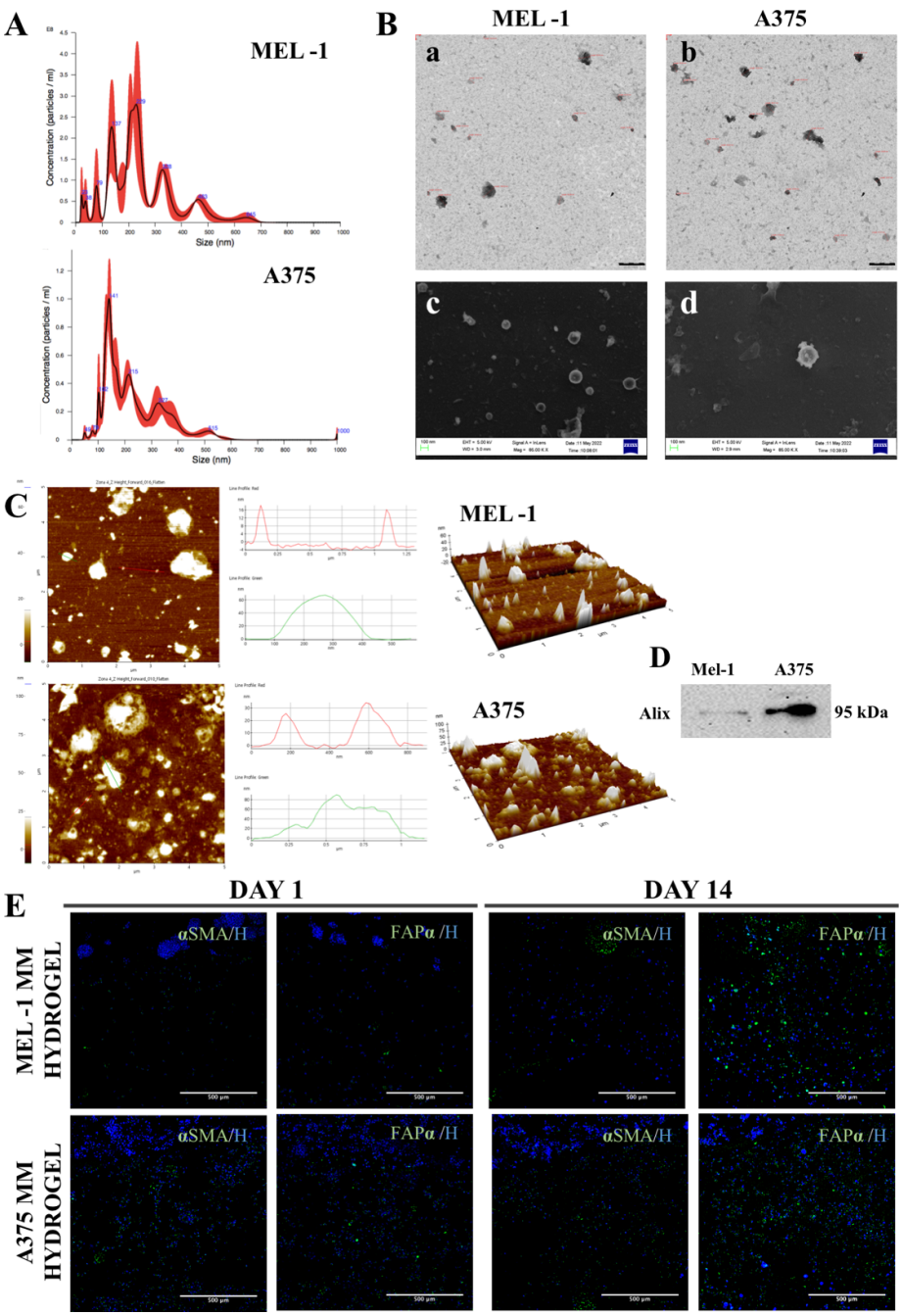

Figure 3. Characterization of A375 and Mel-1MM hydrogel cells inner communication. (A)–(D) Characterization of EVs and exosomes isolated from conditioned media from MM hydrogels. (A) EVs Size distribution analyzed by NTA. (B) TEM (a), (b) and SEM (c), (d) images of isolated EVs with a round shape. (C) Topography of EVs observed under AFM. Acquisition area of 5 μm^2. (D) WB analysis of Alix exosomal surface marker. (E) Confocal representative images at days 1 and 14 of FBs within MM hydrogel stained with αSMA and FAPα antibodies. Scale bar: 500 μm.

enables cell extravasation and metastasis. To study the induction of vasculature in the MM hydrogel, HUVECs and FBs co-cultured in spheroids were bioprinted on the dermal layer, as it has been shown that 3D structures improve the development of vascularization in *in vitro* models [27], and long-term stability of vasculature structures can be enhanced by including FBs [27, 28]. Spheroids were generated using the hanging-drop technique, where the HUVECs form the nucleus of the spheroid, while the FBs are arranged in the second layer (figure 4(A)). HUVECs and CSCs were stained with CTR dye and FBs and MSCs with CTG dye, to easily trace the spatial disposition of the cells. In figure 4(B) it can be seen that on the first day of culture the HUVECs-FBS spheroids showed more compact, while on day 3 cells can be seen migrating from the spheroids, suggesting initial attempts of a vascularization process.

Moreover, in the MM hydrogels it was not necessary the supplementation of VEGF when including

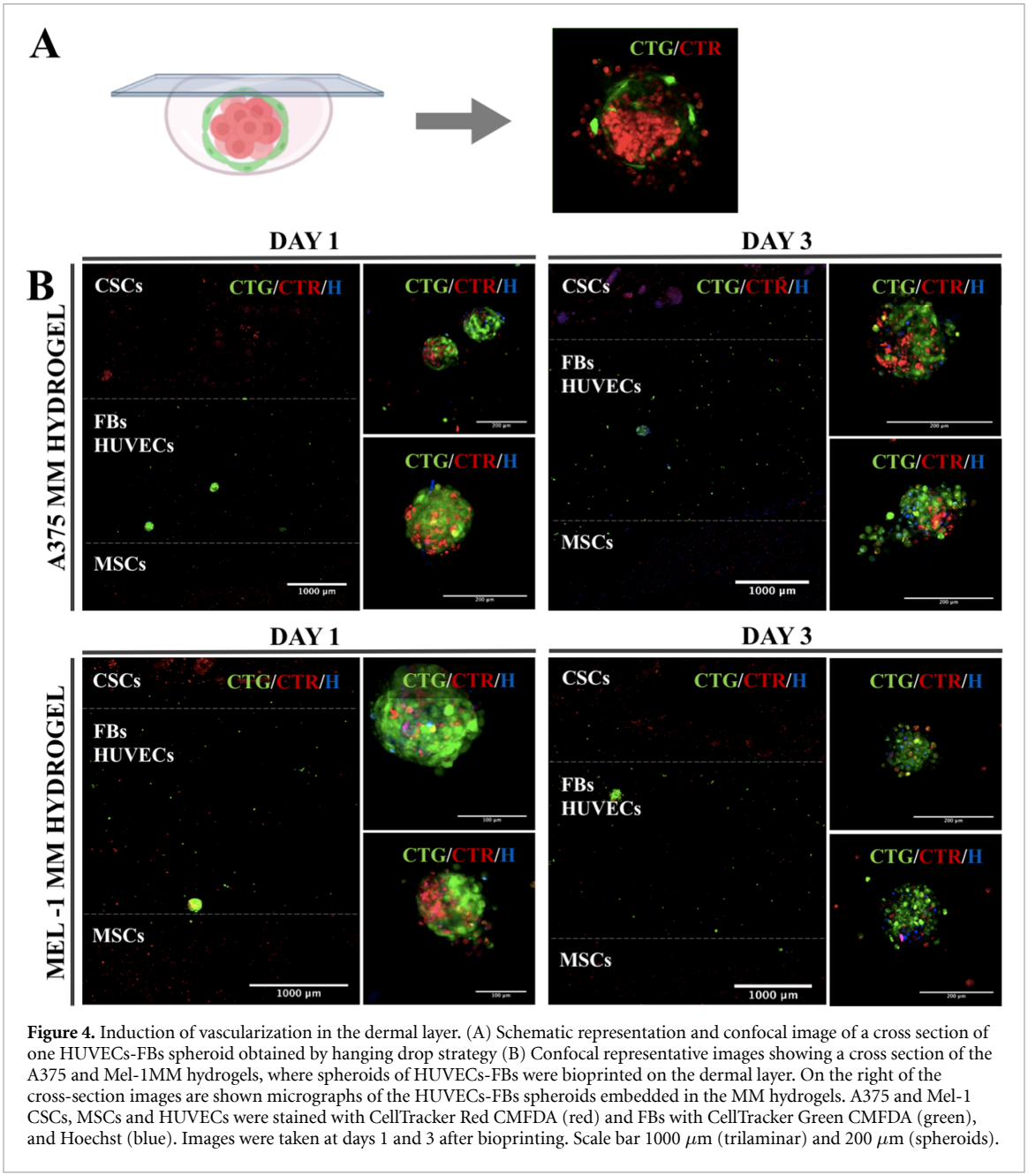

Figure 4. Induction of vascularization in the dermal layer. (A) Schematic representation and confocal image of a cross section of one HUVECs-FBs spheroid obtained by hanging drop strategy (B) Confocal representative images showing a cross section of the A375 and Mel-1MM hydrogels, where spheroids of HUVECs-FBs were bioprinted on the dermal layer. On the right of the cross-section images are shown micrographs of the HUVECs-FBs spheroids embedded in the MM hydrogels. A375 and Mel-1 CSCs, MSCs and HUVECs were stained with CellTracker Red CMFDA (red) and FBs with CellTracker Green CMFDA (green), and Hoechst (blue). Images were taken at days 1 and 3 after bioprinting. Scale bar 1000 μm (trilaminar) and 200 μm (spheroids).

HUVECs co-cultured with FBs in the dermal layer, as HUVECs, FBs and CSCs expressed VEGF in hydrogels cultured in VEGF-free medium, suggesting a cross-talk between that cell types (see supplementary material, figure S7).

3.6. Incorporation of KTCs in the epidermal layer

The epidermal layer of the skin is basically composed of KTCs, which are crucial for the functions of skin tissue. Therefore, in order to achieve a more biomimetic model, KTCs were included in the epidermal layer together with the MM CSCs (figure 5). As can be seen in figure 5 the MM hydrogels are stable over 14 days and cell viability did not decrease for the three layers ($p > 0.05$). Moreover, a significant increase of cell proliferation was observed over two weeks ($^{***}p < 0.005$). These results indicate that KTCs were not affected in their viability and proliferation when they are encapsulated within the 3D bioprinted MM hydrogels.

3.7. Antitumor drug response of CSCs-loaded and MM hydrogels

Autologous models have shown high potential as a key step between research and clinical practice, as they can allow greater prediction of treatment success. Therefore, we tested the effect of VMF, a widely used drug for the treatment of MM patients, in the A375 and Mel-1MM hydrogels. This drug was chosen since both A375 and Mel-1 cell lines are BRAF mutated (figure S3). Increasing doses of VMF were administered every 24 h on CSCs melanospheres cultured in suspension and on CSCs-loaded hydrogels, and cellular proliferation was tested after 24 and 48 h

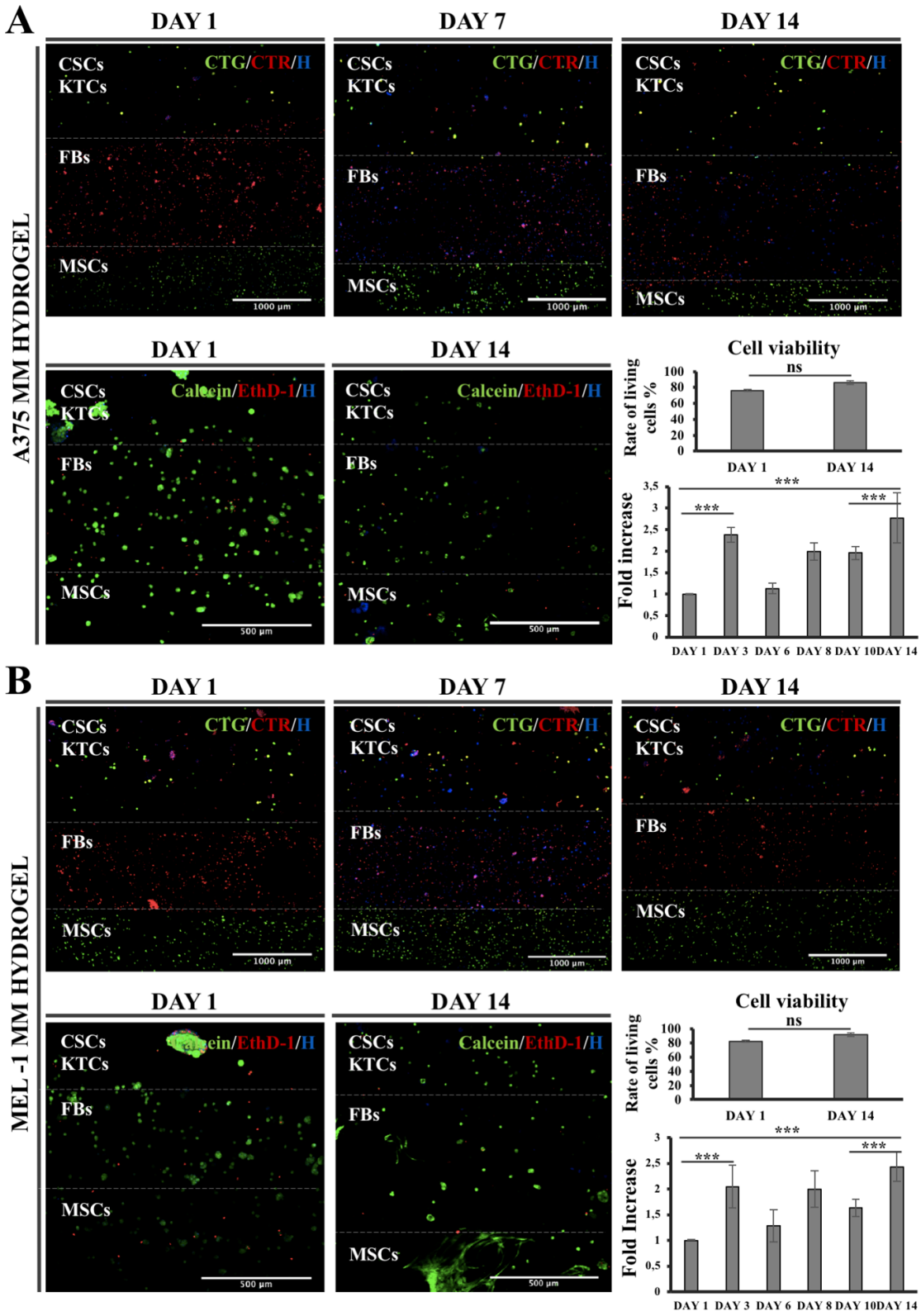

Figure 5. Cellular structure, viability and proliferation analysis of the MM hydrogels including keratinocytes. Confocal representative images obtained by confocal microscopy showing a cross-section of the A375 (A) and Mel-1 (B) MM hydrogels after 1, 7 and 14 days in culture. CSCs and MSCs were stained with CellTracker Green CMFDA (green) and KTCs and FBs were stained with CellTracker Red CMFDA (red) and Hoechst (blue). Below are shown the cross-section images at days 1 and 14 of the MM hydrogels for (A) A375- and (B) Mel-1-based models. Live cells are shown in green (Calcein) and dead cells in red (EthD-1). Scale bar: 500 μm. Graphics on the top right show quantification of live/dead cells at days 1 and 14 with no significant difference on living cells fraction ($n = 4$; $p > 0.05$). Graphics on the bottom right show fold change of proliferation of cells embedded in the trilaminar hydrogels at days 1, 3, 6, 8, 10 and 14 ($n = 4$; $p < 0.005$).

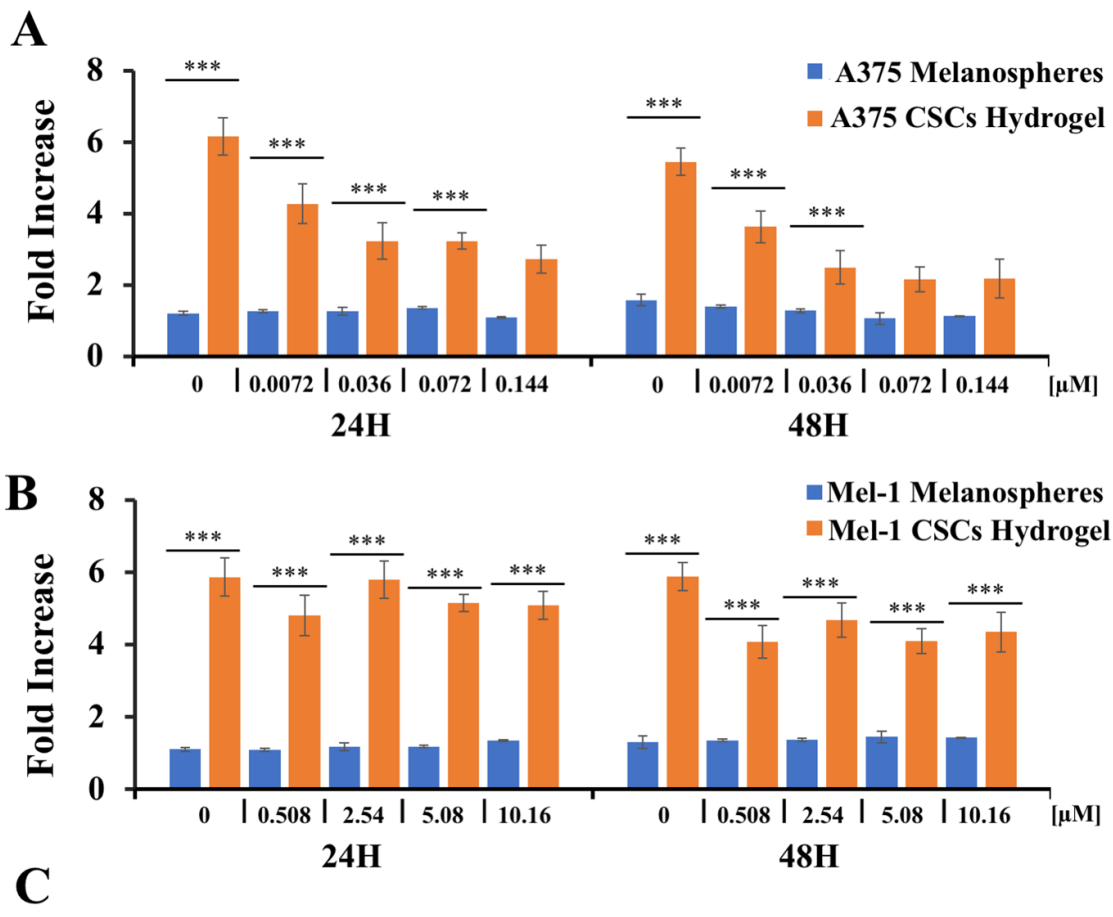

C

		A375					Mel-1			
		24h		48h			24h		48h	
		CSCs Hydrogel	Melano-spheres	CSCs Hydrogel	Melano-spheres		CSCs Hydrogel	Melano-spheres	CSCs Hydrogel	Melano-spheres
P-value	0.0072μM	0.07	0.45	**0.03**	0.35	0.508μM	0.11	0.81	0.11	0.76
P-value	0.036μM	**0.01**	0.69	**0.00**	0.16	2.54μM	0.94	0.50	0.40	0.70
P-value	0.072 μM	**0.00**	0.11	**0.00**	0.06	5.08μM	0.47	0.31	0.22	0.47
P-value	0.144μM	**0.00**	0.17	**0.00**	0.05	10.16μM	0.41	**0.02**	0.26	0.54

Figure 6. Cytotoxic effect of vemurafenib in MM CSCs cultured as melanospheres in suspension and in the CSCs-loaded hydrogel. Graphics show fold change of proliferation of A375 (A) and Mel-1 (B) CSCs cultured in suspension or CSCs-loaded hydrogels after treatment with increasing doses of VMF for 24 and 48 h ($n = 4$; $p < 0.005$). (C) Fold changes and *P*-values corresponding to graphics. *P*-values in bold indicate statistical significance.

(figure 6). To additionally study the effect of the drug on healthy cells included in the model, the higher VMF dose was tested in MM hydrogels, refreshing the treatment each 24 h. MM hydrogel cell viability was measured at 24, 48, and 72 h with the Live/Dead kit (figure 7).

For the A375 melanospheres and CSCs-loaded hydrogels, the drug concentrations applied were 0 μM, 0.0072 μM, 0.036 μM, 0.072 μM and 0.144 μM (figure 6(A)). In both non-treated and treated samples, CSCs proliferation significantly increased in CSCs-loaded hydrogels in comparison to melanospheres suspension cell culture at 24 and 48 h (figures 6(A) and S8). For CSCs-loaded hydrogels the proliferation ratio decreased in a dose-dependent manner, whereas for CSCs cultured in suspension the lower dose (0.0072 μM) inhibited the growth rate, and an increase of the dose did not significantly improve the anti-tumor response (figures 6(C) and S8).

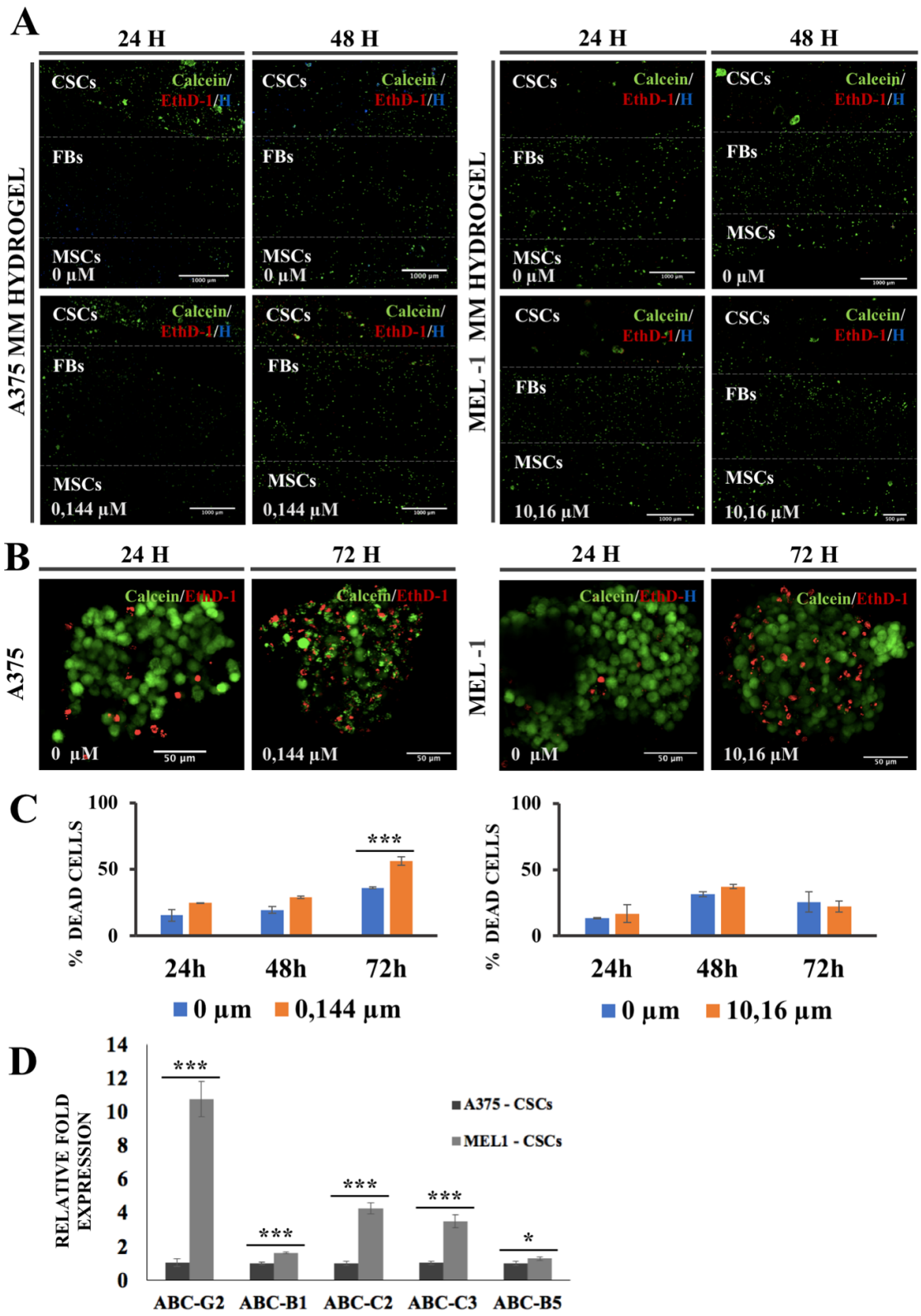

Figure 7. Cytotoxic effect of vemurafenib in MM hydrogels. (A) Confocal representative images showing a cross-section of the A375 and Mel-1 MM hydrogels after 24 and 48 h in culture with different VMF doses: 0 μM, 0.144 μM (A375) and 0 μM, 10.16 μM (Mel-1). Scale bar: 1000 μm. (B) Micrographs of the A375 or Mel-1 CSCs after 72 h in culture with different VMF doses: 0 μM, 0.144 μM (A375) and 0 μM, 10.16 μM (Mel-1). Scale bar: 500 μm. Live cells are shown in green (Calcein) and dead cells in red (EthD-1). (C) Graphics show quantification of live/dead CSCs percent at 24, 48 and 72 h of both non-treated control and MM hydrogels treated with high doses of VMF: 0.144 μM (A375) and 10.16 μM (Mel-1), respectively ($n = 4$). (D) Graphics show expression of ABCG2, ABCB1, ABCC2, ABCC3 and ABCB5 genes measured by qPCR of A375 and Mel-1 CSCs.

Furthermore, the viability assay demonstrated that the A375 MM hydrogel showed the antitumor effect of VMF on CSCs (figure 7). In the dermal and hypodermal layers, it was observed a strong viability marking (green), so FBs and MSCs viability was not affected by the drug treatment (figure 7(A)). In addition, a significant increase in the percentage of dead A375 CSCs was observed at 72 h of treatment with 0.144 μM VMF, with values up to approximately 50% with respect to the drug-free control (figures 7(B) and (C)).

On the other hand, for the Mel-1 melanospheres and CSCs-loaded hydrogels the concentrations of drug applied were 0 μM, 0.508 μM, 2.54 μM, 5.08 μM, and 10.16 μM (figure 6(B)). Similarly to the A375 CSCs-loaded hydrogel, a greater proliferation of CSCs in both non-treated and treated hydrogels was also observed in comparison to melanospheres cultured in suspension (figures 6(B) and S9). But contrarily to the A375 CSCs-loaded hydrogel, no significant differences were found between non-treated and treated samples either 24 or 48 h after bioprinting (figures 6(C) and S9). Furthermore, there was no a significant decrease in the percentage of dead tumor cells at 24, 48, and 72 h with respect to day 0 and the drug-free control Mel-1MM hydrogels, and it remains approximately below 30%–40% in all cases (figure 7(C)). These results indicate that VMF, even at high doses, did not compromise cell viability and proliferation for Mel-1 CSCs.

Finally, the expression of genes related to chemoresistance was analyzed to explore the differences in VMF response between both MM lines. The expression of ABCG2, ABCB1, ABCC2, ABCC3 and ABCB5 genes, from ABC transporters family widely described for MM drug resistance [29] was measured by qPCR (figure 7(D)). A slight but significant increase in the expression of ABCB1, ABCC2, ABCC3 and ABCB5 was observed in Mel-1 with respect to A375 CSCs. In the case of ABCG2, there was a remarkable increased expression in Mel-1 CSCs compared to A375 CSCs ($^{***}p < 0.005$).

3.8. Establishment of *in vivo* subcutaneous MM models

In order to evaluate the tumorigenic potential and the preservation of tumor structure and microenvironment of the hydrogels, MM hydrogels (loading CSCs, FBs, HUVECs and MSCs) and CSCs-loaded hydrogels were subcutaneously implanted in NSG mice. The same number of CSCs inoculated with Matrigel was used as a control, as the conventional model for generating tumors *in vivo*. The MM and CSCs-loaded hydrogels were maintained 14 days in culture before implantation in the murine model.

In all cases, an increase in tumor volume was observed (figure 8(A)), but while the implanted hydrogels experienced more gradual growth, the Matrigel control underwent much faster growth, resulting in significantly larger tumors after 34 days post-inoculation. Moreover, the MM hydrogels exhibited a more regular appearance than the controls. In addition, after implantation, the MM hydrogels presented a larger size, which increased slightly in the first week and stabilized until one month later. On the contrary, for CSCs-loaded hydrogels, the first measurement showed a smaller size, probably due to the hydrogel degradation activity by the tumor cells prior to implantation, which was also observed in rheology assays (figures 3(D) and (E)), and the tumor grew gradually until day 34.

After 34 days, all animals were sacrificed and the tumors were excised for immunofluorescence and histochemical analysis. Microscopic examination of representative histopathological of tumor tissue sections was made staining with Masson's Trichrome, Van Gieson's Trichrome (figure 8) and Hematoxylin-Eosin (figure S9). In the MM hydrogel a layered structure could be distinguished, where the tumoral and stromal stratums had been kept clearly separated (figure S9), whereas in the CSCs-loaded hydrogels and control models a more homogeneous composition was observed. In addition, in the MM hydrogel, remnants of the bioink can be observed in the stromal layer, which appears faintly stained between the cells, while in the CSCs-loaded hydrogel it had almost completely disintegrated. Remarkably, highly dense spherical structures were observed in the upper layer of MM hydrogel and CSCs-loaded hydrogel, with cells within them (figures 8(B) and S9), similar in appearance to melanocyte nests present in this native tumor type. Additionally, the expression of ABCB5, CD44, VEGF, αSMA, and FAPα (figure 8) and human-HLA (figure S9) was analyzed in all tumor models, with special attention to the nest-like structures. The CSCs-loaded hydrogel and Matrigel controls showed heterogeneity in ABCB5 and CD44 staining. However, ABCB5 was not observed in the stromal layer of the MM hydrogel, but it was expressed in the upper layer, in the nest-like structures, while CD44 was expressed in both the stromal and tumor layers. Similarly, VEGF was expressed in all samples, emphasizing the robust vascularization surrounding both hydrogel tumor models. αSMA and FAPα markers were also expressed in all conditions but appeared considerably more marked in the stromal layer of the MM hydrogel, evidencing the malignification of the stromal cells. Finally, the expression of human-HLA was higher in MM hydrogels (figure S9), showed a higher maintenance of the human cells that formed the tumor before the *in vivo* assay. Therefore, these results indicate that the MM hydrogel model more closely maintains and recreates the human tumor TME, both in structure and composition, resulting

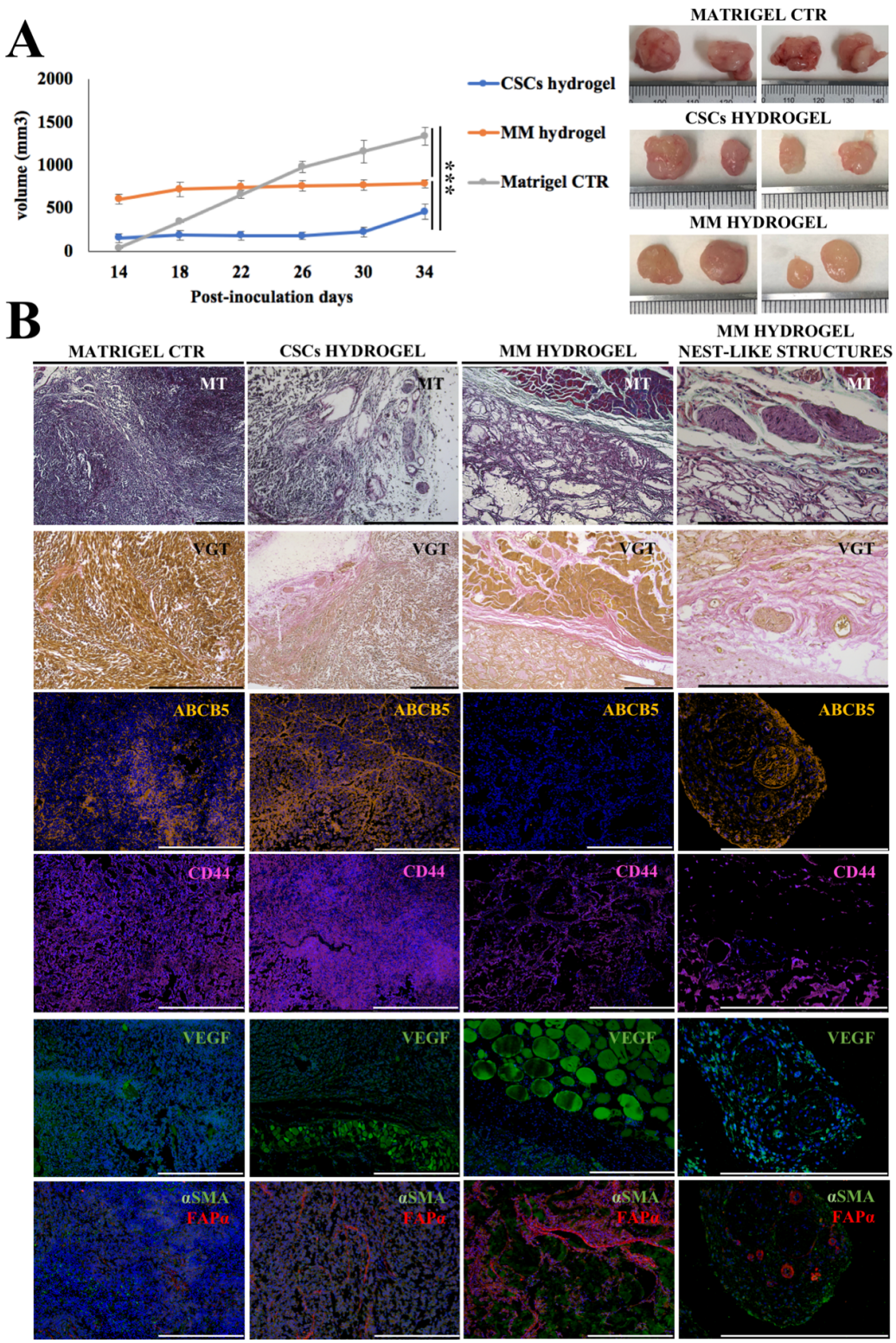

Figure 8. *In vivo* analysis of tumorigenic potential of MM hydrogel and CSCs-loaded hydrogel. (A) MM hydrogel and CSCs-loaded hydrogel xenograft tumor development compared with CSCs injection in NSG mice. Graphic shows mean tumor volume over time ($n = 6$). Adjacent, representative images of excised tumors 34 days after implantation. (B) Representative panel of histology (Masson's Trichrome and Van Gieson's Trichrome) and immunofluorescence staining for ABCB5, CD44, VEGF, αSMA and FAPα expression in paraffin and OCT sections of xenograft tumors 34 days after CSCs inoculation or MM and CSCs-loaded hydrogels implantation. Magnification 5× and 10×. On the right, amplification of melanocytes nest-like structures from MM hydrogel (20×). Scale bar 500 μm.

in the formation of melanocyte nest-like structures in the apical layer of the construct.

4. Discussion

Understanding the underlying biology of tumor initiation and progression is the first step to successful progress in the development of new and efficient cancer therapies. In recent years, cancer research has shown the need to develop new tumor models more biomimetic, since interactions between cells, TME and ECM are key factors in the tumorigenic process, which lead tumor proliferation, angiogenesis, metastasis and condition the response to treatments. In this context, biofabrication technologies such as 3D bioprinting emerges as a new tool that allows representing the complex tumor heterogeneity and mimics the native tumor structure[1]. In this study, we have 3D bioprinted a MM hydrogel, with a three-layered structure that comprises CSCs, the initiating cells of a tumor, and KTCs for the epidermal layer, FBs and ECs for the dermal layer and MSCs for the hypodermal layer, resembling its structure and composition with the *in vivo* model of MM. Moreover, we used two different BRAF mutated MM cell types, an established cell line (A375) and a primary patient-derived cell line (Mel-1), to determine differences in sensitivity of the MM hydrogels to VMF treatment.

For bioprinting the MM equivalent, an adequate bioink formulation was designed to faithfully recreate the ECM. Collagen type I, a major component of normal skin, is the most commonly used material to generate a matrix for skin and melanoma 3D modeling [11], as it supports cell attachment, migration and allows growth and function of several cells types [14, 15]. For the improvement of its mechanical and printable properties, it was combined with agarose, since it allows to acquire the required shape and consistency [30], and does not interfere with cell viability and proliferation [31]. In addition, the combination of agarose with collagen has been shown to induce differentiation of MSCs to adipocytes [32], which constitutes the bulk of the skin hypodermal tissue. On the other hand, the culture conditions for the MM hydrogel were also optimized to accurately represent tumor heterogeneity and an appropriate balance in the rate of CSCs. Interestingly, A375 tumor cells embedded in the MM hydrogels maintained a more stem-like state after 14 days in culture than Mel-1 (22–24). These results agree with the MM hydrogels proliferation rates, in which it is noted that Mel-1MM hydrogels have a higher growth rate than those loaded with A375, an indicator of cell differentiation since stem cells are characterized by a lower proliferation (4).

The bioprinted hydrogels maintained its structure at least for 14 days, and gelled immediately after printing, a crucial characteristic for the formulation of a bioink [7], and to maintain a clearly organized three-layered structure. Extrusion-based bioprinting used in this study is the optimal for viscose hydrogels with high cell density [14]. However, it could result an aggressive procedure due to diverse factors such as the hydrogel composition or the process itself [9]. Furthermore, high agarose concentration could interfere in CSCs proliferation, as it increases gel density and solid stress that inhibits spheroid growth [33]. Nonetheless, in our bioprinted constructs viability and proliferation assays demonstrated an adequate nutrient diffusion into the hydrogels, as well as no adverse effects of the bioink and the bioprinting process. Moreover, ESEM analysis confirmed that cells maintained a high metabolic activity. In addition, diverse biological processes were observed such as cell divisions and the production of ECM and EVs, whose characteristics discard apoptotic process, as they measured less than 500 nm and showed homogeneous appearance [34]. Cells displayed a round morphology and established communication with each other through their exosomes and microvesicles (80–500 nm), which are involved in processes as relevant as TME dynamics and remodeling, fibroblast activation, organotropic metastasis, angiogenesis, and drug resistance [35]. Analysis of the conditioned medium of MM hydrogels by different techniques confirmed the presence of these EVs and exosomes, positive for Alix labeling [25]. In addition, fibroblast activation was confirmed by the phenotypic change of the fibroblasts, expressing FAPα and αSMA markers. The expression levels of both markers can be related to a tumoral phenotype, but they have extremely heterogeneous expression patterns and vary widely between different subpopulations of CAFs [26, 36], so while there is currently no consensus on universal CAF markers, these results do demonstrate that there is a phenotypic shift of FBs in the MM hydrogel and, thus, a communication network between different cell types in the TME.

During tumor progression ECM suffers relevant variations in terms of structure and composition, which impact on mechanical properties of the TME [37, 38]. In this study, changes in the viscoelastic and compression modulus along time reflected the MM hydrogels' remodeling effect on the ECM, since the bioprinted hydrogels significantly vary only in tumorigenic conditions, especially those containing only the CSCs layer. These findings support that CSCs participate actively in the matrix remodelation by inducing fast degradation of the hydrogel. CSCs secrete proteolytic enzymes to facilitate cells growth, cancerous matrix deposition and metastasis [4, 37, 39], which changes the cell–cell adhesion force and subsequently the mechanical properties of the tissue [40]. Moreover, CSCs induce the ECM proteolytic remodeling by stroma cells [4]. On the other hand, CSCs also participates in the assemble of new cancerous matrix with greater physical properties than healthy matrix

[41], as suggested by the raised values in viscoelastic moduli, in agreement with other studies [42, 43], and the ECM deposition observed in the ESEM analysis.

Furthermore, due to the importance of blood vessel structures for tumor hallmarks, metastatic process and chemotherapeutics delivery to solid tumors [2], vascular ECs were included in the MM hydrogels. For that, HUVECs-FBs spheroids were bioprinted in the dermal layer, which seemed to initiate early attempts of migration in the hydrogels. In concordance with previous works, we also observed a secretion of VEGF by CSCs and FBs, suggesting a cross-talk with HUVECs [44, 45]. Moreover, VEGF participates also in an autocrine signaling in CSCs, promoting cell stemness and self-renewal [46], and CSCs can also perform new branched vessels, in a process called vascular mimicry, guided by soluble factors from the TME [47, 48]. The development of vascularized tumor models involves an important step on cancer research, since not even *in vivo* models can completely recreate tumorigenic vessels, as tumors in murine models grow faster than human tumors, and their immature blood vessels are not comparable with long-term established human ones [49].

To date, preclinical models fail to recapitulate the tumor heterogeneity, and animal models neither predict what actually happens in humans [50]. Furthermore, in the clinical practice, the variability between patients makes it difficult to predict the response to drugs and side effects [51], so autologous tumor models have been proposed as a powerful strategy to achieve more accurate results. Here, the effect of VMF was tested in both BRAF mutated A375 and Mel-1MM hydrogels. In the case of A375, it was observed that the hydrogel provided greater drug resistance and promoted cell proliferation [10], in line with other studies that compare the chemotherapeutic effect in 3D and 2D tumor models [52, 53]. However, the Mel-1 CSCs-loaded hydrogel did not respond positively to the drug, for any of the doses applied, nor was its cellular viability affected. Although both cell lines present the same mutation for BRAF (V600E), which should sensitize them for this treatment, this study supports that they respond differently. These contradictory results might be explained by the different origins (established and primary patient-derived cell lines) and the acquired resistance level for both MM cell types. Previously, it has been demonstrated that BRAF mutant A375 cell line is sensitive to VMF [54], which agrees with the dependant doses response found in our A375 CSC-based model. In contrast, the non-response to high doses of VMF in the Mel-1 CSCs-loaded hydrogel is attributable to the acquired resistance of CSCs isolated of this primary patient-derived MM cell line. In fact, despite the clinical success of VMF in the increase of progression-free survival in MM patients, most patients have tumor-recurrence with drug-resistant disease within 6–8 months [55, 56]. In the expression analysis of genes related to chemoresistance, a significant overexpression of ABCG2, ABCB1, ABCC2, ABCC3 and ABCB5 genes, members of the ABC transporters family, was demonstrated in the patient-derived MM line compared to the established one. These genes, especially ABCG2 and ABCB5, are widely associated with acquired resistance to VMF, mainly for MM [57–60]. In fact, a novel preclinical trial has studied the effect of ABCB1/ABCG2 inhibitor to sensitize tumor lines to VMF treatment, suggesting a significant improvement in the therapeutic efficacy [61]. Nonetheless, it has been shown that the effect of VMF can additionally depend on post-translational modifications or multiple alternative ways of acquiring resistance [62, 63], that could also explain the altered Mel-1 CSCs response to VMF. All these results indicate that our MM hydrogels are able to sensibly detecting different response to drug treatment depending of tumor characteristics and have a great potential to predict treatment efficacy in accordance with the individual response variability among patients to the same therapeutic regime.

In addition, the MM hydrogels demonstrated tumorigenesis capacity *in vivo* with a more representative growth rate, structure, and composition, which would allow more comprehensive studies of pharmacological response since our model biomimics the bulk tumor heterogeneity including interactions between cells and TME. As demonstrated by staining of tumor sections, a stratified structure was maintained in the MM hydrogel, with an upper layer comprising tumor cells and structures similar to the melanocytes nest present in human melanoma, and a bottom layer with stromal cells, positive for CD44, αSMA and FAPα markers, but negative for ABCB5, characteristic of MM CSCs and differentiated tumor cells [64]. Expression of CD44, αSMA, and specifically FAPα on stromal cells in TME is linked to environmental malignancy and generation of the CSCs niche [65, 66]. In addition, the presence, size, and appearance of the melanocyte nests can be clinically useful as diagnostic and classification criteria of MM [67–69] On the other hand, positive expression of human HLA demonstrates a low substitution of mouse cells in the tumor model, a major concern currently associated with PDX models [70]. Moreover, VEGF labeling shows consistent vascularization of hydrogel-based tumor models, a fundamental factor for pharmacological diffusion of new compounds studies. This more robust angiogenesis is probably due to the fact that slower tumor growth favors the generation of more stable vessels, whereas the faster growth linked to conventional tumor cell injection models results in more fragile vessels in response to the exponential nutrient and oxygen demand of the tumor [49]. Therefore, the histopathological characteristics of the *in vivo* tumor from MM hydrogel resemble human tumor features and biochemical context, providing a more sophisticated and realistic

platform for the investigation of novel oncological treatments. This may be crucial for the study of new drugs that do not target tumor cells, but other components of TME. In fact, there is a multitude of new anti-tumor treatments proposed, many of them being tested in clinical trials, that target stromal cells, the vasculature, the tumor's own extracellular matrix [71], and even the intercellular communication networks occurring in the TME [4, 71]. However, most of the classical animal models used for preclinical screening of antitumor drugs include only one cell type and, in several cases, while a drug shows excellent antitumor properties *in vivo*, it proves to be ineffective in clinical trials, and therefore unable to be translated into clinical practice. Therefore, more reliable models that are able to incorporate both human cells and the complete physiology of an *in vivo* model are proposed as a promising tool for screening these new therapies [72, 73].

5. Conclusions

To our knowledge, it is the first time that a novel 3D bioprinted MM hydrogel has been developed, simulating both MM skin structure and TME. When implanted in NSG mice, it allows the generation of biomimetic xenograft models recreating similar structure and composition that human tumor bulk. However, our model comprises only an initial vascularization, without achieving a more complex vascular network, and immune system is not yet fully included in this type of platforms. Despite these limitations, this MM hydrogel provides a promising *in vitro* and *in vivo* platform for the detailed study of molecular pathways and tumor components interaction. Moreover, this system has a high potential for high throughput anticancer drug screening campaigns targeted against MM and, more important, to the optimization of current MM treatments towards a precision and personalized medicine more reliable and successful to improve quality of life and treatment response in MM patients. Finally, this MM hydrogel could be a fundamental step between animal testing and clinical trials, reducing the need for laboratory animals and giving more consistent data about drug pharmacology, which will result in lots of time and resources savings.

Data availability statement

All data that support the findings of this study are included within the article (and any supplementary files).

Acknowledgments

Thanks to Juan de Vicente for his work and assessment with rheometer. Also we thanks Ana María Santos Caro, Mohamed Tassi Mzanzil, Concepción Hernández Castillo, and Isabel Sanchez Almazo, Jaime Lazuen Alcón and Jose Manuel Entrena Fernández from the C I C (Universidad de Granada) for their technical assistance.

Author contributions

J L A and G J G conception and design, collection and/or assembly of data, data analysis and interpretation, manuscript writing. M R T, C C W, C A A, C G L, and E L R collection and/or assembly of data. J A M conception and design, data analysis and interpretation.

Funding

This work was supported by grants from Consejería de Salud y Familias de la Junta de Andalucía (Project No. PIN-0224-2019), by the Consejería de Economía, Conocimiento, Empresas y Universidad de la Junta de Andalucía (FEDER Funds, Projects PY18-FR-2470, B-CTS-230-UGR18, A-CTS-180-UGR20, PYC20 RE 015 UGR and P18-FR-2465), by the Ministry de Economía y Competitividad, Instituto de Salud Carlos III (FEDER funds, Projects Nos. DTS19/00145 and DTS21/00098), and from the Chair 'Doctors Galera-Requena in cancer stem cell research' (CMC-CTS963). Funding for open access charge: Universidad de Granada/CBUA. G J acknowledges the posdoctoral fellowship from Plan Andaluz de Investigación, Desarrollo e Innovación (PAIDI 2020—FEDER funds—Ref: DOC_01574). All figures were created with Biorender.com.

Conflict of interest

The authors confirm that there are no known conflicts of interest associated with this publication.

ORCID iD

Juan Antonio Marchal https://orcid.org/0000-0002-4996-8261

References

[1] Zhang Y S, Duchamp M, Oklu R, Ellisen L W, Langer R and Khademhosseini A 2016 Bioprinting the cancer microenvironment *ACS Biomater. Sci. Eng.* **2** 1710–21
[2] Hui L and Chen Y 2015 Tumor microenvironment: sanctuary of the devil *Cancer Lett.* **368** 7–13
[3] Kenny P A, Lee G Y and Bissell M J 2007 Targeting the tumor microenvironment *Front. Biosci.* **1** 3468–74
[4] López de Andrés J, Griñán-Lisón C, Jiménez G and Marchal J A 2020 Cancer stem cell secretome in the tumor microenvironment: a key point for an effective personalized cancer treatment *J. Hematol. Oncol.* **13** 136
[5] Knowlton S, Onal S, Yu C H, Zhao J J and Tasoglu S 2015 Bioprinting for cancer research *Trends Biotechnol.* **33** 504–13
[6] Junttila M R and De Sauvage F J 2013 Influence of tumour micro-environment heterogeneity on therapeutic response *Nature* **501** 346–54

[7] Mandrycky C, Wang Z, Kim K and Kim D-H 2016 3D bioprinting for engineering complex tissues *Biotechnol. Adv.* **34** 422–34
[8] Murphy S V, Skardal A and Atala A 2012 Evaluation of hydrogels for bio-printing applications *J. Biomed. Mater. Res.* A **101** 272–84
[9] Guvendiren M, Molde J, Soares R M D and Kohn J 2017 Designing biomaterials for 3D printing *ACS Biomater. Sci. Eng.* **2** 1679–93
[10] Dababneh A B and Ozbolat I T 2014 Bioprinting technology: a current state-of-the-art review *J. Manuf. Sci. Eng.* **136** 061016
[11] Hotary K B, Allen E D, Brooks P C, Datta N S, Long M W and Weiss S J 2003 Membrane type I matrix metalloproteinase usurps tumor growth control imposed by the three-dimensional extracellular matrix *Cell* **114** 33–45
[12] Vultur A, Schanstra T and Herlyn M 2016 The promise of 3D skin and melanoma cell bioprinting *Melanoma Res.* **26** 205–6
[13] Zhou X, Zhu W, Nowicki M, Miao S, Cui H, Holmes B, Glazer R I and Zhang L G 2016 3D bioprinting a cell-laden bone matrix for breast cancer metastasis study *ACS Appl. Mater. Interfaces* **8** 30017–26
[14] Jeong S-Y, Lee J-H, Shin Y, Chung S, Kuh H-J and Lee J W 2016 Co-culture of tumor spheroids and fibroblasts in a collagen matrix-incorporated microfluidic chip mimics reciprocal activation in solid tumor microenvironment *PLoS One* **11** e0159013
[15] Glowacki J and Mizuno S 2008 Collagen scaffolds for tissue engineering *Biopolymers* **89** 338–44
[16] Rao S S, DeJesus J, Short A R, Otero J J, Sarkar A and Winter J O 2013 Glioblastoma behaviors in three-dimensional collagen-hyaluronan composite hydrogels *ACS Appl. Mater. Interfaces* **9** 9276–84
[17] Velasco D, Quílez C, Garcia M, Del Cañizo J F and Jorcano J L 2018 3D human skin bioprinting: a view from the bio side *J. 3D Print. Med.* **2** 141–62
[18] Pourchet L J *et al* 2017 Human skin 3D bioprinting using scaffold-free approach *Adv. Healthcare Mater.* **6** 1601101
[19] Cubo N, Garcia M, Del Cañizo J F, Velasco D and Jorcano J L 2016 3D bioprinting of functional human skin: production and *in vivo* analysis *Biofabrication* **9** 015006
[20] Memic A, Navaei A, Mirani B, Cordova J A V, Aldhahri M, Dolatshahi-Pirouz A, Akbari M and Nikkhah M 2017 Bioprinting technologies for disease modeling *Biotechnol. Lett.* **39** 1279–90
[21] Dominici M, Le Blanc K, Mueller I, Slaper-Cortenbach I, Marini F C, Krause D S, Deans R J, Keating A, Prockop D J and Horwitz E M 2006 Minimal criteria for defining multipotent mesenchymal stromal cells. The international society for cellular therapy position statement *Cytotherapy* **8** 315–7
[22] Erfani E, Roudi R, Rakhshan A, Sabet M N, Shariftabrizi A and Madjd Z 2016 Comparative expression analysis of putative cancer stem cell markers CD44 and ALDH1A1 in various skin cancer subtypes *Int. J. Biol. Markers* **31** 53–61
[23] Thapa R and Wilson G D 2016 The importance of CD44 as a stem cell biomarker and therapeutic target in cancer *Stem Cells Int.* **2016** 2087204
[24] Zhang S, Yang Z and Qi F 2020 Aldehyde dehydrogenase-positive melanoma stem cells in tumorigenesis, drug resistance and anti-neoplastic immunotherapy *Mol. Biol. Rep.* **47** 1435–43
[25] Willms E *et al* 2016 Cells release subpopulations of exosomes with distinct molecular and biological properties *Sci. Rep.* **6** 22519
[26] Gonda T A, Varro A, Wang T C and Tycko B 2010 Molecular biology of cancer-associated fibroblasts: can these cells be targeted in anti-cancer therapy? *Semin. Cell Dev. Biol.* **21** 2–10
[27] Wenger A, Kowalewski N, Stahl A, Mehlhorn A T, Schmal H, Stark G B and Finkenzeller G 2006 Development and characterization of a spheroidal coculture model of endothelial cells and fibroblasts for improving angiogenesis in tissue engineering *Cells Tissues Organs* **181** 80–88
[28] Newman A C, Nakatsu M N, Chou W, Gershon P D and Hughes C C W 2011 The requirement for fibroblasts in angiogenesis: fibroblast-derived matrix proteins are essential for endothelial cell lumen formation *Mol. Biol. Cell* **22** 3791–800
[29] Böhme I, Schönherr R, Eberle J and Bosserhoff A K 2021 Membrane transporters and channels in melanoma *Rev. Physiol. Biochem. Pharmacol.* **181** 269–374
[30] Varoni E, Tschon M, Palazzo B, Nitti P, Martini L and Rimondini L 2012 Agarose gel as biomaterial or scaffold for implantation surgery: characterization, histological and histomorphometric study on soft tissue response *Connect. Tissue Res.* **53** 584–54
[31] Miguel S P, Ribeiro M P, Brancal H, Coutinho P and Correia I J 2014 Thermoresponsive chitosan-agarose hydrogel for skin regeneration *Carbohydrate Polym.* **111** 366–73
[32] Duarte Campos D F, Blaeser A, Korsten A, Neuss S, Jäkel J, Vogt M and Fischer H 2015 The stiffness and structure of three-dimensional printed hydrogels direct the differentiation of mesenchymal stromal cells toward adipogenic and osteogenic lineages *Tissue Eng.* A **21** 740–56
[33] Helmlinger G, Netti P A, Lichtenbeld H C, Melder R J and Jain R K 1997 Solid stress inhibits the growth of multicellular tumor spheroids *Nat. Biotechnol.* **15** 778–83
[34] El Andaloussi S, Mäger I, Breakefield X O and Wood M J A 2013 Extracellular vesicles: biology and emerging therapeutic opportunities *Nat. Rev. Drug Discov.* **12** 347–57
[35] Mashouri L, Yousefi H, Aref A R, Ahadi A M, Molaei F and Alahari S K 2019 Exosomes: composition, biogenesis, and mechanisms in cancer metastasis and drug resistance *Mol. Cancer* **18** 75
[36] Nurmik M, Ullmann P, Rodriguez F, Haan S and Letellier E 2020 In search of definitions: cancer-associated fibroblasts and their markers *Int. J. Cancer* **146** 895–905
[37] Mierke C T 2011 The biomechanical properties of 3D extracellular matrices and embedded cells regulate the invasiveness of cancer cells *Cell Biochem. Biophys.* **61** 217–36
[38] Ng M R and Brugge J S 2009 A stiff blow from the stroma: collagen crosslinking drives tumor progression *Cancer Cell* **16** 455–7
[39] Brábek J, Mierke C T, Rösel D, Veselý P and Fabry B 2010 The role of the tissue microenvironment in the regulation of cancer cell motility and invasion *Cell Commun. Signal.* **8** 8
[40] Mierke C T 2014 The fundamental role of mechanical properties in the progression of cancer disease and inflammation *Rep. Prog. Phys.* **77** 076602
[41] Mittal S, Brown N J and Holen I 2018 The breast tumor microenvironment: role in cancer development, progression and response to therapy *Expert Rev. Mol. Diagn.* **18** 227–43
[42] Malik R, Lelkes P I and Cukierman E 2015 Biomechanical and biochemical remodeling of stromal extracellular matrix in cancer *Trends Biotechnol.* **33** 230–6
[43] Oskarsson T 2013 Extracellular matrix components in breast cancer progression and metastasis *Breast* **22** S66–S72
[44] Black A F, Berthod F, L'heureux N, Germain L and Auger F A 1998 *In vitro* reconstruction of a human capillary-like network in a tissue-engineered skin equivalent *FASEB J.* **12** 1331–40
[45] Sewell-Loftin M K *et al* 2017 Cancer-associated fibroblasts support vascular growth through mechanical force *Sci. Rep.* **7** 12574
[46] Hamerlik P *et al* 2012 Autocrine VEGF-VEGFR2-Neuropilin-1 signaling promotes glioma stem-like cell viability and tumor growth *J. Exp. Med.* **209** 507–20
[47] Ricci-Vitiani L *et al* 2010 Tumour vascularization via endothelial differentiation of glioblastoma stem-like cells *Nature* **468** 824–30

[48] Bussolati B, Grange C, Sapino A and Camussi G 2009 Endothelial cell differentiation of human breast tumour stem/progenitor cells *J. Cell. Mol. Med.* **13** 309–19
[49] Song H H G, Park K M and Gerecht S 2014 Hydrogels to model 3D *in vitro* microenvironment of tumor vascularization *Adv. Drug Deliv. Rev.* **79–80** 19–29
[50] Unger C *et al* 2014 Modeling human carcinomas: physiologically relevant 3D models to improve anti-cancer drug development *Adv. Drug Deliv. Rev.* **79–80** 50–67
[51] Santo V E, Rebelo S P, Estrada M F, Alves P M, Boghaert E and Brito C 2017 Drug screening in 3D *in vitro* tumor models: overcoming current pitfalls of efficacy read-outs *Biotechnol. J.* **12** 1600505
[52] Dunne L W, Huang Z, Meng W, Fan X, Zhang N, Zhang Q and An Z 2014 Human decellularized adipose tissue scaffold as a model for breast cancer cell growth and drug treatments *Biomaterials* **35** 4940–9
[53] Liu C, Lewin Mejia D, Chiang B, Luker K E and Luker G D 2018 Hybrid collagen alginate hydrogel as a platform for 3D tumor spheroid invasion *Acta Biomater.* **75** 213–25
[54] Zhao K, Lu Y, Chen Y, Cheng J and Zhang W 2020 Transcripts 202 and 205 of IL-6 confer resistance to Vemurafenib by reactivating the MAPK pathway in BRAF (V600E) mutant melanoma cells *Exp. Cell Res.* **390** 111942
[55] Schadendorf D, van Akkooi A C J, Berking C, Griewank K G, Gutzmer R, Hauschild A, Stang A, Roesch A and Ugurel S 2018 Melanoma *Lancet* **392** 971–84
[56] Sosman J A *et al* 2012 Survival in BRAF V600–mutant advanced melanoma treated with vemurafenib *New Engl. J. Med.* **366** 707–14
[57] Marzagalli M, Raimondi M, Fontana F, Montagnani Marelli M, Moretti R M and Limonta P 2019 Cellular and molecular biology of cancer stem cells in melanoma: possible therapeutic implications *Semin. Cancer Biol.* **59** 221–35
[58] Wu C-P, Sim H-M, Huang Y-H, Liu Y-C, Hsiao S-H, Cheng H-W, Li Y-Q, Ambudkar S V and Hsu S-C 2013 Overexpression of ATP-binding cassette transporter ABCG2 as a potential mechanism of acquired resistance to vemurafenib in BRAF(V600E) mutant cancer cells *Biochem. Pharmacol.* **85** 325–34
[59] Wu C-P and Ambudkar S 2014 The pharmacological impact of ATP-binding cassette drug transporters on vemurafenib-based therapy *Acta Pharm. Sin.* B **4** 105–11
[60] Monzani E *et al* 2007 Melanoma contains CD133 and ABCG2 positive cells with enhanced tumourigenic potential *Eur. J. Cancer* **43** 935–46
[61] Durmus S, Sparidans R W, Wagenaar E, Beijnen J H and Schinkel A H 2012 Oral availability and brain penetration of the B-RAFV600E inhibitor vemurafenib can be enhanced by the P-GLYCOprotein (ABCB1) and breast cancer resistance protein (ABCG2) inhibitor elacridar *Mol. Pharm.* **9** 3236–45
[62] Díaz-Martínez M, Benito-Jardón L, Alonso L, Koetz-Ploch L, Hernando E and Teixidó J 2018 miR-204-5p and miR-211-5p contribute to BRAF inhibitor resistance in melanoma *Cancer Res.* **78** 1017–30
[63] Torres-Collado A X, Knott J and Jazirehi A R 2018 Reversal of resistance in targeted therapy of metastatic melanoma: lessons learned from vemurafenib (BRAFV600E-specific inhibitor) *Cancers* **10** 157
[64] Setia N, Abbas O, Sousa Y, Garb J L and Mahalingam M 2012 Profiling of ABC transporters ABCB5, ABCF2 and nestin-positive stem cells in nevi, *in situ* and invasive melanoma *Mod. Pathol.* **25** 1169–75
[65] Kinugasa Y, Matsui T and Takakura N 2014 CD44 expressed on cancer-associated fibroblasts is a functional molecule supporting the stemness and drug resistance of malignant cancer cells in the tumor microenvironment *Stem Cells* **32** 145–56
[66] Liu T, Han C, Wang S, Fang P, Ma Z, Xu L and Yin R 2019 Cancer-associated fibroblasts: an emerging target of anti-cancer immunotherapy *J. Hematol. Oncol.* **12** 86
[67] Kutzner H *et al* 2012 Histological and genetic evidence for a variant of superficial spreading melanoma composed predominantly of large nests *Mod. Pathol.* **25** 838–45
[68] Leecy T N *et al* 2020 Large nested melanoma: a clinicopathological, morphometric and cytogenetic study of 12 cases *Pathology* **52** 431–8
[69] Viros A *et al* 2008 Improving melanoma classification by integrating genetic and morphologic features *PLoS Med.* **5** e120
[70] Yoshida G J 2020 Applications of patient-derived tumor xenograft models and tumor organoids *J. Hematol. Oncol.* **13** 4
[71] Roma- Rodrigues C, Mendes R, Baptista P V and Fernandes A R 2019 Targeting tumor microenvironment for cancer therapy *Int. J. Mol. Sci.* **20** 840
[72] Schmid R *et al* 2022 A new printable alginate/hyaluronic acid/gelatin hydrogel suitable for biofabrication of *in vitro* and *in vivo* metastatic melanoma models *Adv. Funct. Mater.* **32** 2107993
[73] Grosskopf A K, Correa S, Baillet J, Maikawa C L, Gale E C, Brown R A and Appel E A 2022 Consistent tumorigenesis with self-assembled hydrogels enables high-powered murine cancer studies *Commun. Biol.* **4** 985